energies

MDPI

Article

Enhanced Regenerative Braking Strategies for Electric Vehicles: Dynamic Performance and Potential Analysis

Boyi Xiao [1], Huazhong Lu [1,2,*], Hailin Wang [1], Jiageng Ruan [3] and Nong Zhang [3]

[1] College of Engineering, South China Agricultural University, Guangzhou 510640, China; nickshaw@stu.scau.edu.cn (B.X.) hlwang@scau.edu.cn (H.W.)
[2] Guangdong Academy of Agricultural Sciences, Guangzhou 510640, China
[3] School of Mechanical and Mechatronic Engineering, University of Technology Sydney, 15 Broadway, Ultimo, NSW 2007, Australia; Jiageng.Ruan@uts.edu.au (J.R.); Nong.Zhang@uts.edu.au (N.Z.)
* Correspondence: huazlu@scau.edu.cn; Tel.: +86-138-0887-0688

Received: 13 October 2017; Accepted: 13 November 2017; Published: 15 November 2017

Abstract: A regenerative braking system and hydraulic braking system are used in conjunction in the majority of electric vehicles worldwide. We propose a new regenerative braking distribution strategy that is based on multi-input fuzzy control logic while considering the influences of the battery's state of charge, the brake strength and the motor speed. To verify the braking performance and recovery economy, this strategy was applied to a battery electric vehicle model and compared with two other improved regenerative braking strategies. The performance simulation was performed using standard driving cycles (NEDC, LA92, and JP1015) and a real-world-based urban cycle in China. The tested braking strategies satisfied the general safety requirements of Europe (as specified in ECE-13H), and the emergency braking scenario and economic potential were tested. The simulation results demonstrated the differences in the braking force distribution performance of these three regenerative braking strategies, the feasibility of the braking methods for the proposed driving cycles and the energy economic potential of the three strategies.

Keywords: regenerative braking strategy; energy flow; fuzzy control; battery electric vehicle; driving cycle construction

1. Introduction

The 21st century has witnessed the fast development of battery electric vehicles (BEVs), which provide a favourable solution to global warming and fossil fuel shortages. Relative to conventional cars, a BEV has a higher efficiency of automotive powertrain structure with the capability of bidirectional energy flow for energy management. The bidirectional energy flow enables a vehicle to recapture kinetic energy during deceleration using a regenerative braking system (RBS) without adding any additional components [1].

An RBS is a system that can convert useless kinetic energy into electrical energy for energy reutilization using the electric motor to apply negative torque to the wheels while braking [2]. When driving a conventional vehicle, the potential energy is typically wasted during braking. However, more than 60% of the braking energy can potentially be used in typical urban driving cycles [3]. By adding motor braking to form composite braking, the energy recovery capacity can be significantly enhanced.

The control strategy design of RBSs is substantially more complex than a conventional braking system design. In recent studies of RBSs, scholars worldwide have proposed a series of promising research on RBS strategy designs. In [4], the impact of limiting factors, such as the battery's state of charge (SOC), the characteristics of the battery and motor of a hybrid vehicle RBS, road handling and

stability were investigated. In [5], Oleksowicz et al. examined the European braking regulations for a critical straight braking test using a car simulation. In [6], an energy evaluation management study was proposed: the motor priority strategy was applied to a fuel cell hybrid electric bus for maximum recovery capability, and a fuel economy test was performed, using the HIL test and a road test.

However, the goal of RBS design is to ensure both stable braking performance and efficient energy recovery; however, these two goals have a strong negative correlation in most braking situations [7]. Martin et al. [8] presented a combined braking system, in terms of the damping control of the drive train, and designed a linearized model, which included the tire-road contact. Juan et al. [9] developed a fuzzy RBS strategy using elements like tire forces, vehicle speed and road adhesion for estimation, while considering the wheel slip and braking safety. These works applied simplified braking cycles as the main input. However, real-world-based performance comparisons of regenerative braking strategies, that can fulfil the previously mentioned requirements, are rarely carried out. Therefore, this study is intended to address this deficiency.

In this study, a BEV powertrain model, equipped with an RBS, was completed using Matlab®/Simulink® (VersionR2014a, the Mathworks Co., Natick, MA, USA). The motor dynamic characteristics were tested using a dynamometer, and the battery charging resistance characteristics were obtained from the experimental results. Three braking strategies for an RBS were proposed: the first strategy was a high dynamic strategy that was based on fuzzy control logic, and the second and third strategies were improved versions of common strategies that served as control groups. Energy recovery improvement and braking safety were considered in this study. These braking strategies complied with the ECE-13H braking regulation and passed a straight brake test (emergency braking included) whilst running on typical urban cycles and an experimental cycle for additional economic efficiency demonstration.

1.1. Constraints of Braking Regulations Worldwide

The braking performance and stability tests are integral to conventional vehicles. To proceed with an invalidation test of a vehicle with an RBS system, a general safety braking rule must be considered and followed.

The majority of the regulations in different countries are similar, to ensure uniform vehicle braking safety and efficiency design in all operating circumstances. The European United Nations (UN) Regulation 13-H is the prevalent worldwide standard for light passenger vehicles and light goods vehicles [10]. This regulation is recognized as a legitimate braking standard under the 1958 agreement and is followed by all members of the UN, including Australia, Austria, Japan, Germany, Italy, Switzerland, Norway, the Russian Federation, the United Kingdom (UK), and the United States of America (USA).

According to Economic Commission for Europe(ECE) regulation 13-H, installation of an anti-lock braking system (ABS) in a vehicle is required and must have the supreme priority to take control of vehicle braking in any situation. Similar rules have been promulgated by the United States National Highway Traffic Safety Administration [11]. A vehicle's brake performance should attain the value of a formula-defined brake-strength factor (z). To demonstrate compliance of the proposed regulation, the following BEV regenerative braking procedures were tested, abiding by ECE 13-H:

- Shenzhen driving cycle, NEDC, FTP75, LA92 and JP1015 conditions [12,13].
- Electronic brakeforce distribution (EBD) performance.
- Single straight-line braking with piecewise braking force.
- Energy recovery efficiency test.

1.2. Construction and Comparison of Proposed Driving Cycles

To reproduce typical real-world traffic flow and represent pavement characteristics and driving patterns, a driving cycle is built as a combination of different operating conditions. The cycle is

composed of the acceleration phase, deceleration phase, cruising period, and idle period. Driving cycles are extensively employed as main input values when studying vehicle dynamic performance and energy consumption.

These test cycles include several official and common representations, such as NEDC, FTP75, and LA92. The NEDC is an authoritative "modal" or "polygonal" cycle that consists of artificially constructed micro-tips [14]. In these kinds of micro-trips, values, such as speed and acceleration, are not based on realistic on-road data. Although the NEDC has a high applicability to all types of vehicle tests, its lack of veracity and authenticity when it is applied to diverse settings is concerning. The FTP75 and LA92 cycles are transient driving cycles that are generated from real-time experimental measurements in Los Angeles, USA. These two driving cycles are intended to represent specific traffic conditions and a particular type of vehicle. For a broader reference, the test must contain distinct cycles.

1.3. Development of a Chinese City Driving Cycle

A Chinese city driving cycle for a BEV was constructed, based on real-world experimental results. As a transient cycle, this driving sampling test was conducted in Shenzhen; motor-drive vehicles were the test subjects. The test routes were selected based on the urban passenger traffic demand corridor, which has a high representativeness, and encompasses the central business district (CBD) and residential-industrial areas. Seven routes were selected and tested in both directions for over 200 h, and the road testing direction during different peak periods was considered for accuracy [15]. Three route type clusters were selected: congested road conditions, urban road conditions, and suburban road conditions.

During the speed-time data collection process, to gain high accuracy, a global positioning system (GPS) receiver was installed on the tested vehicles. The step time of the collected GPS data was 0.2 s, and the speed accuracy error was less than ± 0.5 km/h. After the data collection process, all data were segmented into micro-trips. The micro-trip based method has been employed in many experiments by Kamble et al., which confirms its reliability and high efficiency [16]. Each micro-trip contained an idle-acceleration-(cruise)-deceleration-idle circulation, from which an eigenvalue matrix (χ_i) could be calculated. The matrix contained parameters, such as average/maximum speed, average/maximum acceleration, and time proportions of travel series. The mean values (χ_j, j = 1, 2, 3) of the three pre-set route types (low-speed, urban, and suburban) were calculated to obtain an evaluation index. Then, every eigenvalue matrix of the micro-trips was compared with the target evaluation index for data veracity [17], as shown in Equation (1). If the error was 5% or lower, then this micro-trip was selected as a candidate. The comparison ended once all micro-trips had been tested.

$$Error = \left| \frac{\chi_j - \chi_i}{\chi_j} \right| \leq 5\%. \quad (1)$$

Micro-trips were randomly extracted from the three route type clusters and reformed according to the travel time proportion of the original data, namely, 3:4:4. Subsequently, the basic formation underwent a smoothing process, using the Tukey bi-weight kernel method [18] to analyse the simulation and subsequent dynamometer tests. Following the data smoothing process, both the original data and smoothed data were plotted (Figure 1). The majority of the noising sharp sawteeth were eliminated, whereas the velocity characteristics remained. From the speed-time figure, we observe that the composite ShenZhen city driving cycle (SZDC) is composed of a series of low-speed and start-stop profiles, which reveal the actual driving environment in residential, urban, and suburban areas.

A speed characteristic comparison between the SZDC and other mainstream urban cycles is shown in Figure 2. The average speed, running speed (average speed without idle time) and maximum speed are listed. In contrast to other cycles, the SZDC had the lowest maximum speed of 62 km/h, but a high average speed and running speed. This finding indicates that the speed of the SZDC falls

within a narrow range, which corresponds to the urban actuality. By representing these real-world circumstances, an adaptive customized cycle is provided for the following vehicle dynamic simulations.

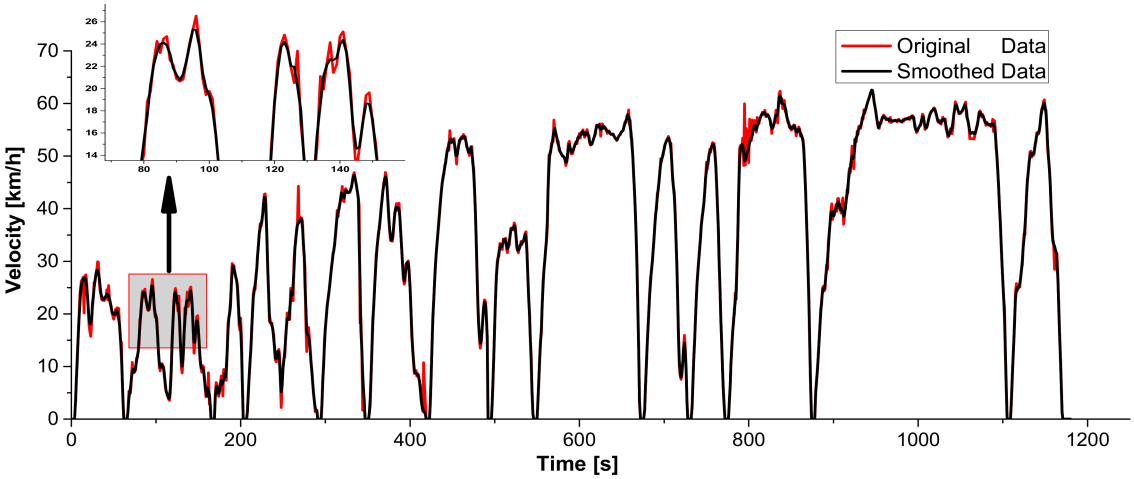

Figure 1. Comparison of ShenZhen city driving cycle (SZDC) original/smoothed velocity data.

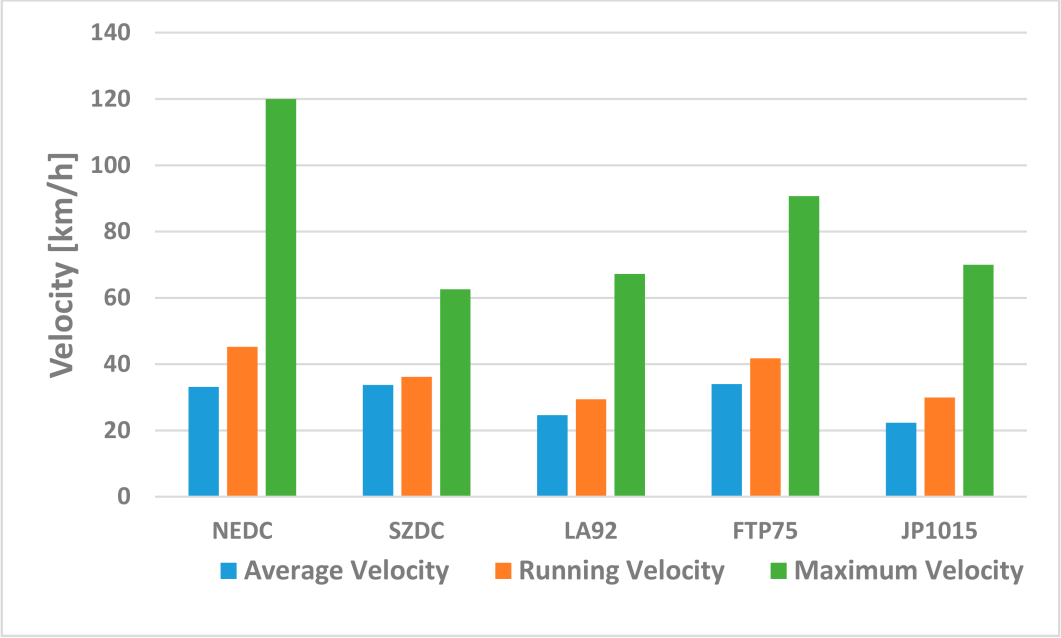

Figure 2. Comparison of velocity among various driving cycles.

2. Powertrain Fundamentals

Figure 3 indicates the topological structure of the BEV platform, which is a front drive type, equipped with both a mechanical hydraulic brake and a motor regenerative brake. The Simulink® model is plotted in Figure 4, which was designed for the performance and safety evaluation of different proposed regenerative braking strategies. In this platform, the battery supports the motor as the main power source. The driver module follows the different driving cycles and presents the acceleration and brake demands. The vehicle control unit (VCU) calculates these demands and transforms them into the commanded brake and drive torque. In the brake torque distribution module, the command brake torque is divided into three values: front motor brake torque (regenerative), front mechanical

brake torque and rear mechanical brake torque. The distribution of brake torque varies across braking strategies, which significantly affects the performance of the RBS.

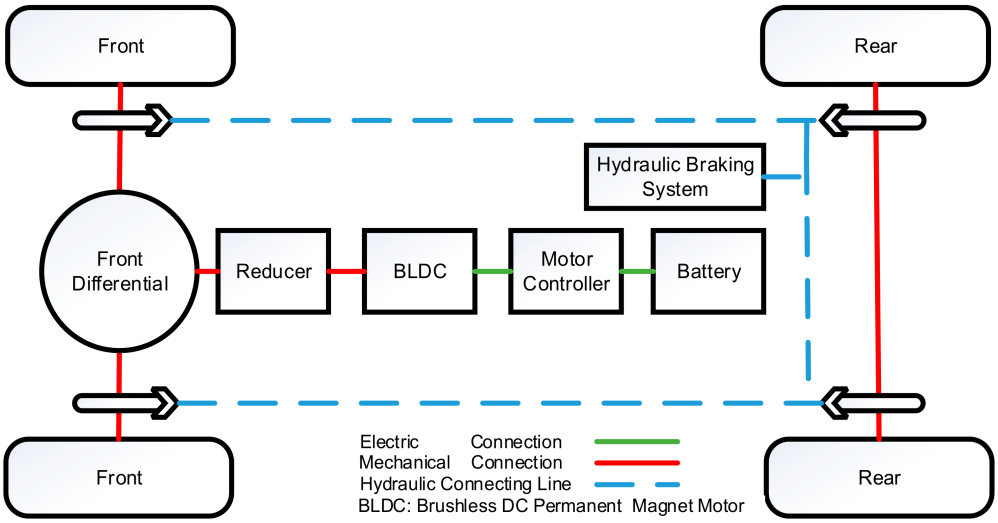

Figure 3. Topological structure of the battery electric vehicles (BEV) platform.

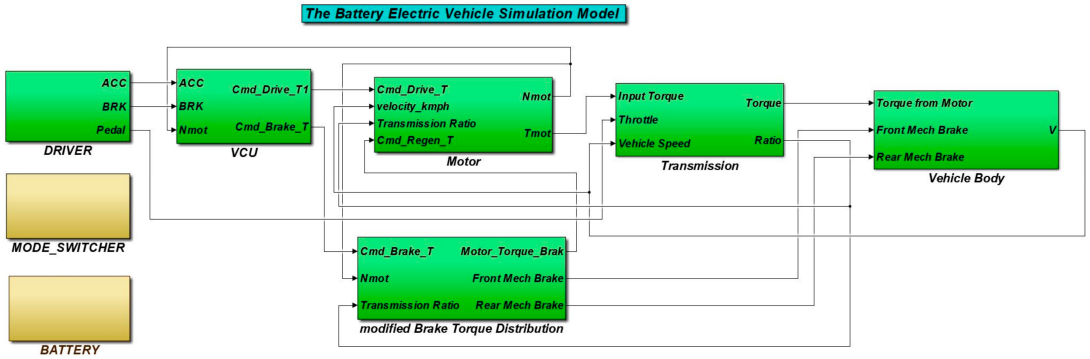

Figure 4. Upper layer of the BEV Simulink® model.

Once the brake torque distribution is set, the motor brake torque goes through the motor module, in which the motor characteristics and limitations are included. In this procedure, the limited motor speed, motor torque and required motor power (driving or regenerating) are solved for the energy consumption during vehicle driving conditions and battery SOC calculations. The detailed model construction will be indicated in the upcoming sections.

2.1. Motor Module

The motor of the powertrain model is used as a drive motor when accelerating and as a generator when regenerative braking is required. During generation, the electric energy is absorbed by the battery. The motor efficiency is based on motor speed and torque, which are the experimental results collected from a brushless DC permanent magnet motor (BLDC) on a vehicle chassis dynamometer. The motor efficiency characteristics are plotted in the three-dimensional diagram in Figure 5.

When a motor is working as generator, the output power is represented as:

$$P_{ren} = \frac{T}{9550N}\eta_{mot}, \quad (2)$$

where P_{ren} represents the recovery power from the motor, T is the motor torque and N is the motor speed. η_{mot} represents the generator efficiency.

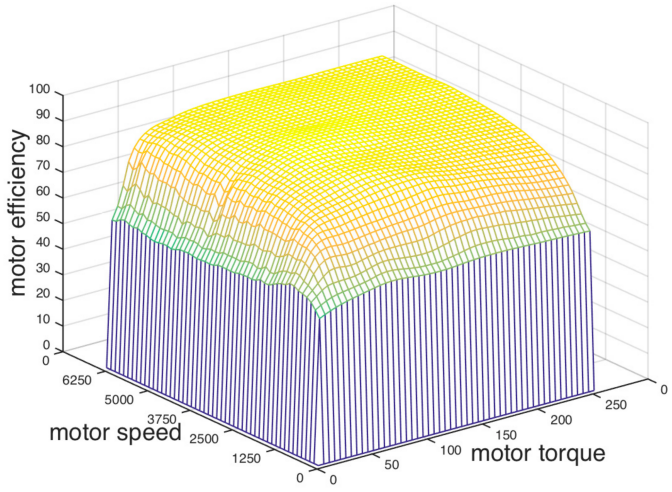

Figure 5. Efficiency characteristics of the BLDC.

2.2. Battery Module

Due to the high energy density and long lifespan, Li-ion batteries have been extensively employed to enable energy storage in electric vehicles [19]. A simplified battery equivalent circuit model was established, based on the electrochemical characteristics from a sampling experiment. The simplified characteristics of the battery voltage and resistance during charging were tested and are shown in Figure 6. In this module, the Li-ion battery charging resistance changes based on the variations of the battery SOC and temperature.

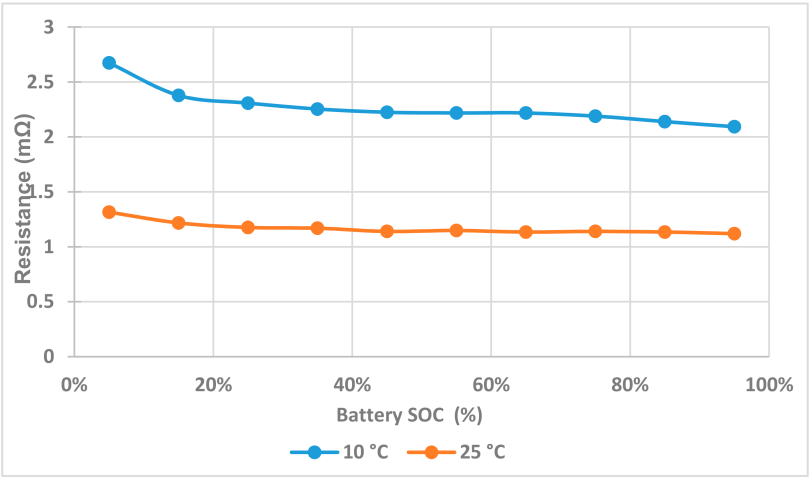

Figure 6. Charging resistance characteristics of a Li-ion battery.

The output energy and input energy of a battery can be calculated using Equations (3) and (4), respectively:

$$E_{bat\_in} = \int_{I_{bat} \leq 0} U_{bat} I_{bat} dt, \tag{3}$$

$$E_{bat\_out} = \int_{I_{bat} > 0} U_{bat} I_{bat} dt. \tag{4}$$

In these integral formulas, U_{bat} and I_{bat} represent the voltage and current of the battery. When $I_{bat} \leq 0$, the battery is charging; otherwise, the battery is discharging. Limitations, such as battery maximum charging/discharging powers, are also included in the module.

2.3. Module of Vehicle Braking Force Distribution

The general braking force distribution of a vehicle is plotted in Figure 7. For electric vehicles with an RBS, the available regenerative braking torque is limited by the motor peak torque [20]. When a braking situation occurs, mechanical braking always supplies the braking torque on the front and rear wheels, whereas the motor is selectively incorporated, based on various strategies and braking situations.

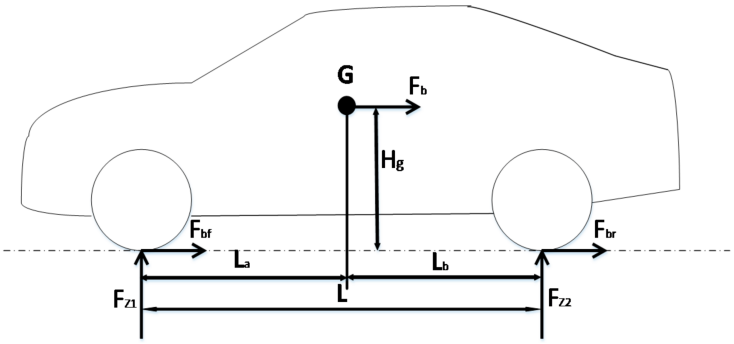

Figure 7. Wheel load analysis when braking on a flat road.

The principle of braking force distribution is based on Equation (5), which represents the relationship between the front wheels and the rear wheels deceleration force:

$$F_b = m\alpha_{dec} = F_{bf} + F_{br}, \tag{5}$$

where m is the mass of the vehicle, α_{dec} is the deceleration of the vehicle, and F_{bf} and F_{br} are the dynamic friction forces of the front tires and rear tires, respectively. The maximum friction forces of the front wheels and rear wheels are calculated using Equations (6) and (7), respectively:

$$F_{bf} = \frac{\mu mg(L_b + zH_g)}{L}, \tag{6}$$

$$F_{br} = \frac{\mu mg(L_a + zH_g)}{L}, \tag{7}$$

where μ is the adhesion parameter on the road surface, L_a and L_b are the distances from the wheel centre to the centre of gravity, g is the acceleration of gravity, and H_g represents the height of the gravity centre.

The blended braking force of the front wheel can be described using Equation (8), which includes the regenerative (motor) braking force and mechanical braking force.

$$F_{bf} = F_{regen} + F_{mechf}. \tag{8}$$

The percentage of motor regenerative braking force in the total front combined braking force is defined as parameter k, which is the regeneration ratio. The value of k is calculated by dividing the regenerative braking force by the front blended braking force, as described in Equation (9).

$$k = \frac{F_{regen}}{F_{regen} + F_{mechf}}. \tag{9}$$

The total braking force (F_{bmax}) is calculated as follows:

$$F_{bmax} = Max\left(F_{bf} + F_{br}\right) = \mu_{max} mg. \tag{10}$$

According to Equation (10), the maximum braking force is limited by the road friction condition. To achieve the maximum braking force from the front tires and rear tires, a special curve ensures maximum stability and controllability in braking, by simultaneously guaranteeing wheel lock on both the front tires and rear tires. This curve is referred to as the ideal braking force distribution curve (I-curve), as follows [21]:

$$F_{br} = \frac{1}{2}\left[\frac{mg}{H_g}\sqrt{L_b + \frac{4H_g}{mg}F_{bf}} - \left(\frac{mgL_b}{H_g} + 2F_{bf}\right)\right]. \tag{11}$$

To estimate the braking load, the braking intensity (z) is introduced, as follows:

$$z = \frac{\alpha_{dec}}{g}. \tag{12}$$

To address braking safety concerns, vehicle manufacturers apply braking regulations, according to the relevant standard. According to European UN Regulation 13-H, wwhen the value of the theoretical adhesion parameter (μ) is between 0.2 and 0.8 for all states of loading (without ABS intervention), the brake strength (z) of two-axle vehicles must satisfy the requirement of Equation (13) [10]:

$$z = \frac{\alpha_{dec}}{g} > 0.1 + 0.70(\mu - 0.2). \tag{13}$$

To achieve a higher demand for braking safety restrictions, the demanding factor (0.70), to which UN Regulation 13-H actually applies, is replaced by a greater margin of safety factor (0.85), which is plotted as the red curve in Figure 8. It is notable that the ideal curve has a higher safety standard than the ECE curve, which has a well-distributed requirement on both axles.

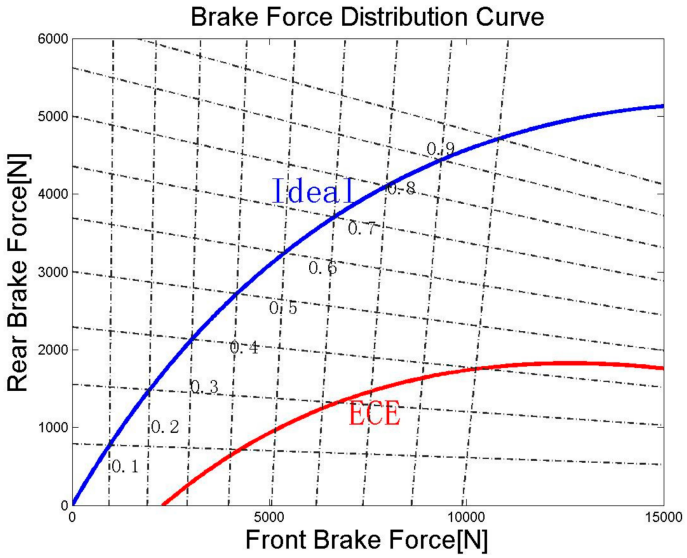

Figure 8. Braking force distribution on the front and rear wheels.

The solid blue curve in the figure represents the "ideal braking force distribution" curve. The design of the braking distribution strategies follows these two curves, to gain a satisfactory balance between braking safety and energy recovery efficiency.

To understand the proposed braking strategies and braking performance concerns, a basic logical flow diagram is shown in Figure 9. When the brake pedal moves, the braking system analyses the brake safety situation and follows the selected braking strategy according to various regulations [10]. Any occurrence of wheel lock triggers the ABS.

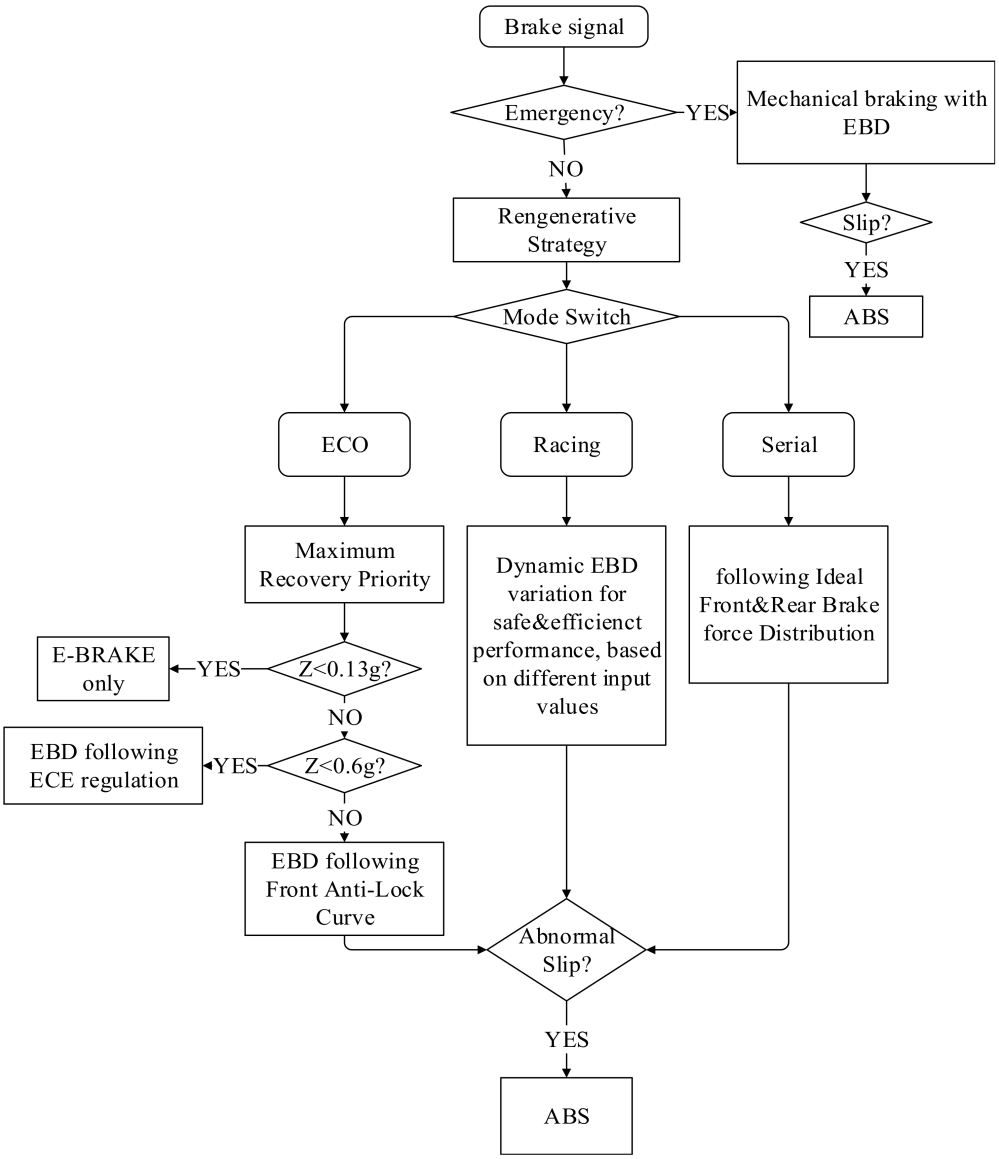

Figure 9. Upper frame of braking strategies for the regenerative braking system (RBS), electronic brakeforce distribution (EBD) and antilock braking system (ABS).

3. Common Regenerative Braking Strategies

3.1. Serial Strategy

The serial strategy presents a well-distributed braking logic. When braking occurs, both front brakes and rear brakes provide a braking force, so as to prevent any possibility of wheel lock. If the brake demand is low, the front braking force is provided by the motor. As the demand continues to increase, the front mechanical braking will be incorporated when the electric braking reaches its maximum capacity. Details of the strategy are shown in Figure 10.

An emergency braking strategy is also presented for the situation of severe braking [10,20]. Once wheel slippage occurs, or the value of brake strength (z) exceeds 0.7, the serial strategy automatically switches to the emergency strategy, in which the distribution of the braking force on the front and rear wheels strictly follows the ideal braking force distribution curve, to maximize brake performance.

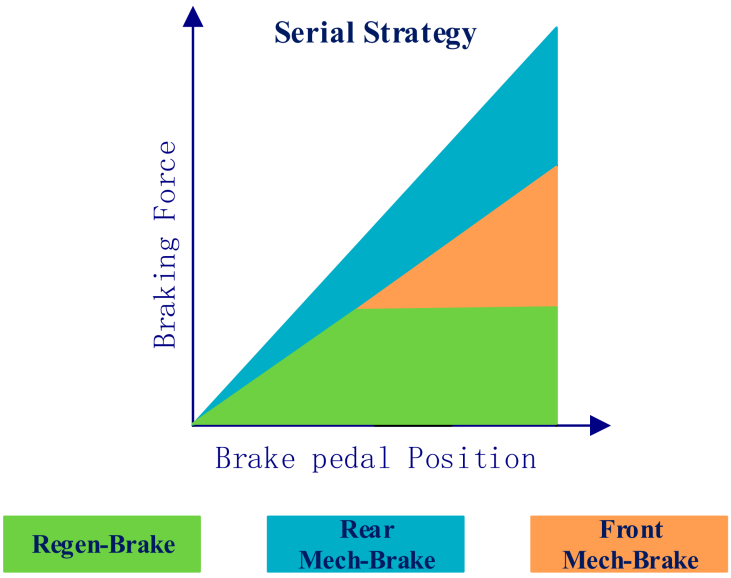

Figure 10. Braking force distribution of serial strategy.

3.2. ECO Strategy

To fully utilize the braking energy, the ecology (ECO) strategy is proposed [20]. This strategy is designed for city cycle situations; only electric motor braking is applied until the motor reaches its maximum capacity. At this intersection point, the mechanical brake starts to involve according to the ECE regulation curve (shown in Figure 11). As the braking deceleration increases and the pre-set emergency value, 0.7, is attained, the ECO strategy will automatically change into an emergency strategy (introduced in Section 3.1). Theoretically, this strategy has the highest energy recovery of all types of regenerative braking; however, its safety and degree of comfort must be considered. As motor braking independently occurs when the brake demand is less than the motor maximum capability, a wheel-lock situation may occur on a low-friction road. A vehicle may lose its steering ability and undergo "oversteering" and "understeering" [22].

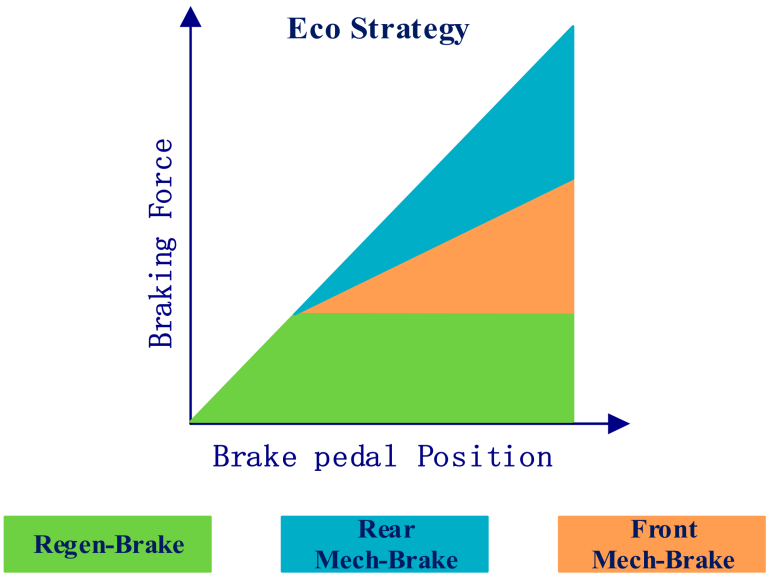

Figure 11. Braking force distribution of the ECO strategy.

3.3. Racing Strategy Based on Fuzzy Logic Distribution

When a higher dynamic power distribution management is needed during driving and braking, the racing strategy is proposed. Due to the limitations of the previous regenerative braking strategies, a vehicle cannot respond to fast and strong brake demands or recover a sufficient amount of energy while driving in rapidly changing velocity conditions. Consequently, the racing strategy must be more responsive and efficient to withstand dangerous situations. This strategy is implemented using a Mamdani fuzzy controller.

Fuzzy control, proposed by Zadeh, in 1965 [23], is a mathematical system that can analyse analogue input values in terms of logical variables. Fuzzy logic operates with discrete values of either 1 or 0 (representing true or false, respectively) [24] and consists of three basic stages: input stage, processing stage and output stage. The input values invoke the rules in the processing stage, evaluate the if-then statements (rules) and generate the results [25].

In a braking system, the vehicle speed has a substantial impact on the stopping distance, which is transformed into the motor spinning speed via ratio conversion. Regarding the braking distribution strategy, the battery SOC and the motor command braking force represent the trend of desired braking distribution. Therefore, these three factors are considered the inputs of the fuzzy controller. The block diagram of the racing strategy is shown in Figure 12, and the influences of these inputs are discussed, as follows.

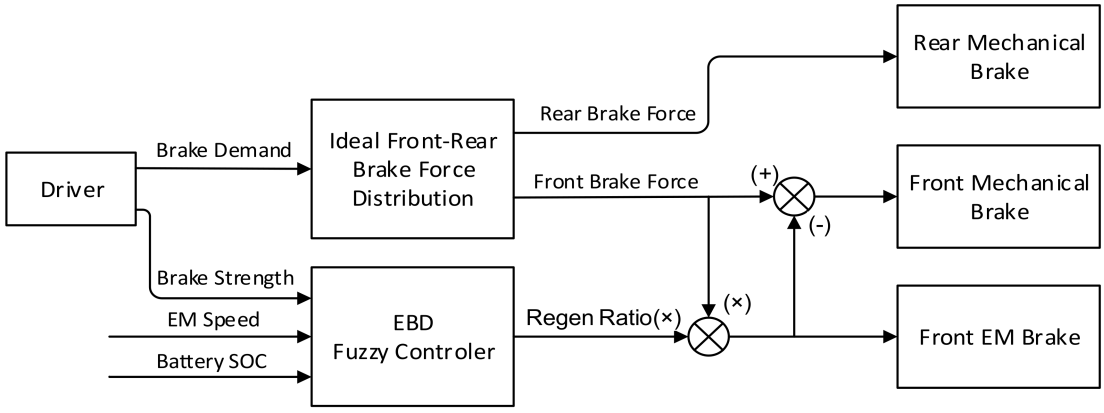

Figure 12. Simplified block diagram of the racing mode control strategy. Note, SOC: state of charge.

The input value "motor speed" has a limited range [0, 6250] [r/min], due to the motor physical properties; this range is divided into three sections: low, middle and high. The membership function of the motor speed is shown in Figure 13a. The motor performance changes gradually with the motor rotation speed, hence, the function, gauss2mf, is selected to prevent abrupt variations. When the motor speed is low, which indicates that the car moves in slow motion and is ready to be stopped by mechanical braking for a more stable constraint, then the ratio of the regenerative braking force is low. When the motor attains a high speed in the medium range, the proportion of the motor braking can increase to the moderate level. When the motor speed is high, the proportion of the regenerative braking force is considered to be high to recycle the massive energy from the high-speed vehicle.

For safety and drive-comfort concerns, the driver's deceleration demand guides the distribution of the RBS. The vehicle deceleration demand is represented by the brake strength (z), whose equation is shown in Equation (13). According to EU-13H, the z factor range is set to [0, 0.8], as shown in Figure 13b. When a low braking force is needed, the motor fulfils most of the brake requirements and provides high energy recovery. Medium braking begins to incorporate mechanical braking. In severe braking, as occurs in emergency braking, the system needs a quick response, so the membership function is designed much more steeply. During this stage, the regenerative braking fades promptly, and the mechanical braking offers the majority of the braking force.

The battery SOC represents the charging state of battery storage. Figure 13c shows the SOC membership functions. When braking in a high-SOC situation, to prevent battery overcharge, the charging current should be limited by having a steeper membership function in the high SOC stage. When the SOC decreases below 80%, the battery can accommodate a higher current; thus, the proportion of regenerative braking can increase to a medium level. When the SOC is lower than 30%, the proportion of motor braking participation should increase to a high level to charge additional power to prevent the battery from excessive discharges.

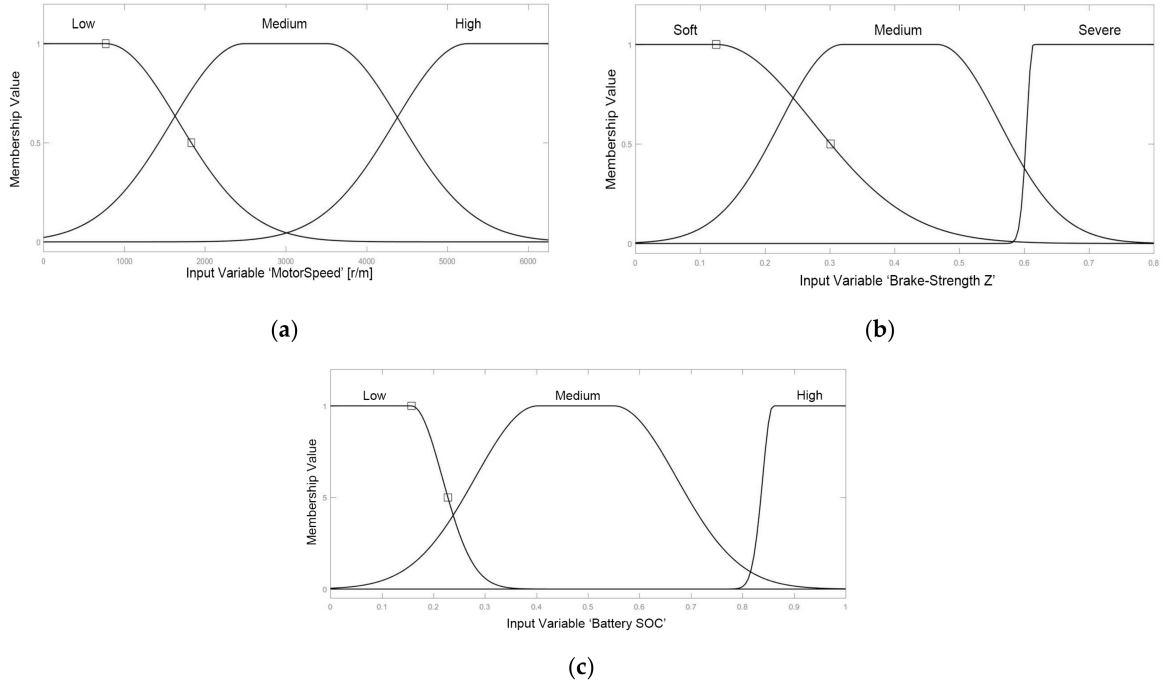

Figure 13. (**a**) Membership function of the motor speed. (**b**) Membership function of the brake strength (*z*). (**c**) Membership function of the battery SOC.

The only output of the fuzzy controller is the regenerative braking distribution ratio (k). The range of this ratio (k) is [0, 1], which is the regenerative force's proportion of the front wheel braking force, as characterized by Equation (9) in Section 2.2. The regeneration ratio (k) varies according to the features of the inputs and rules. To obtain k from the fuzzy controller output, the centre of gravity method is taken as the mapping defuzzification approach. However, some undesirable effects, such as fluctuations, may occur as this method does not have interpolation properties. To avoid these negative effects, the fuzzy output is described as a single value for each rule, and its weighted mean is assigned to the crisp output value, "k_i", in the conclusion [24]. The equation of this algorithm is expressed as follows:

$$k = \left(\sum_{i=1}^{n} \beta_i k_i \right) / \sum_{i=1}^{n} \beta_i \tag{14}$$

where k_i represents the value of the ith rule on the total output, β_i is the output of the ith rule, and k is the defuzzified system output.

The output surface of the fuzzy inference RBS controller is plotted in Figure 14, which shows the relationships between input values and the output regeneration ratio (k). The battery SOC, deceleration strength and motor speed have detectable and rational influences on the output, thus satisfying the expectation of the pre-set rules and demonstrating the validity of the fuzzy control strategy.

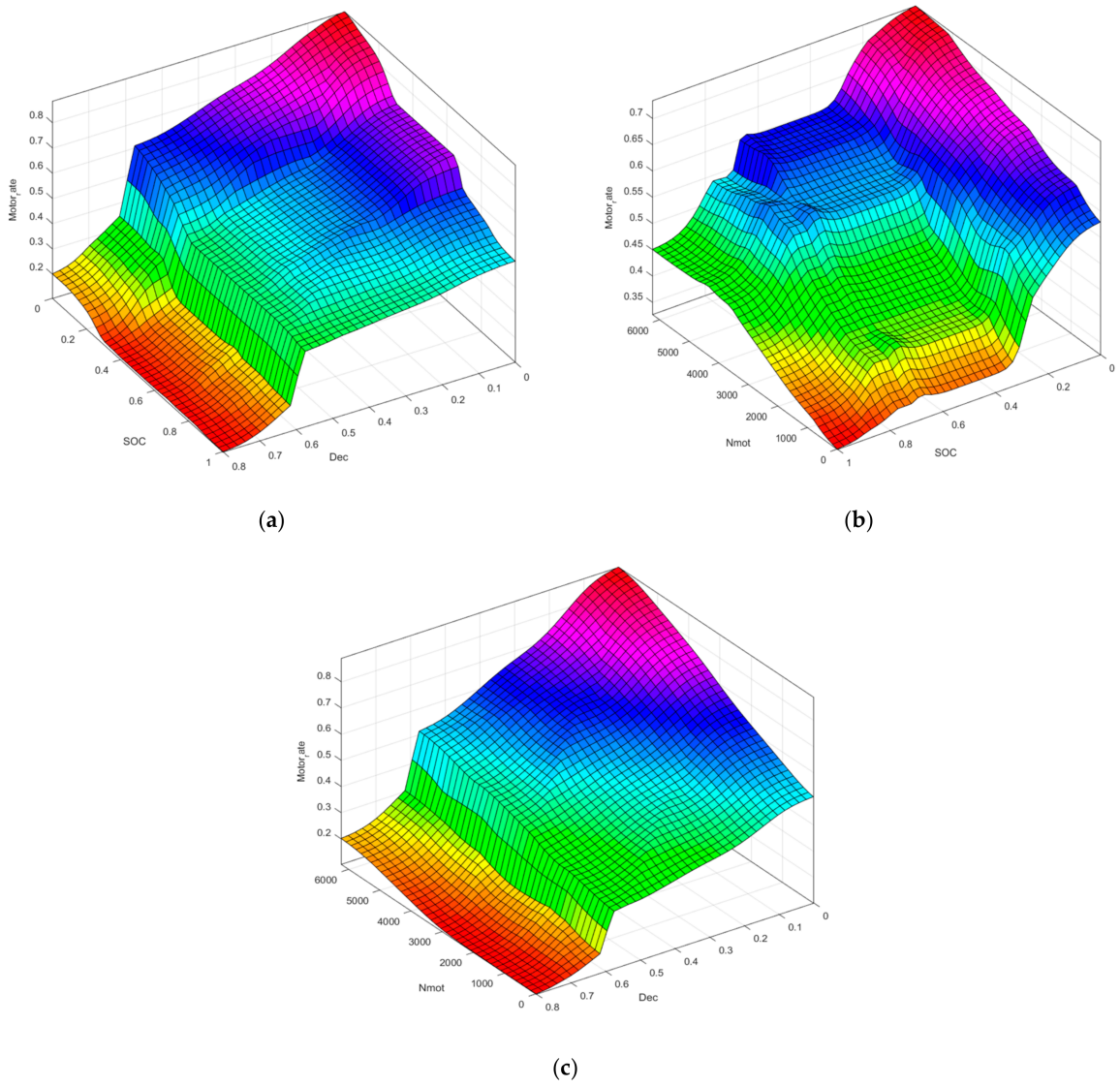

Figure 14. Braking distribution ratio (k) relationships among different inputs; (**a**) relationship with motor speed; (**b**) relationship with deceleration strength; (**c**) relationship with battery SOC.

4. Dynamic Performance and Energy Recovery Analysis

The aim of RBS design was to achieve higher energy recovery, while maintaining manoeuvrability and stability. Two tests were performed: the straight braking performance test and the driving cycle economic test.

4.1. Straight Braking Test

As shown in Figure 15, a multi-stage straight braking cycle was used to test the dynamic performance of various proposed strategies. In this cycle, the brake test started at 100 km/h, the vehicle began to decelerate to 95 km/h in 2 s, and the speed decelerated from 95 km/h to 60 km/h in 3 s and stopped in 3.5 s. The deceleration was classified into three stages, based on the brake strength: soft (51–53 s, 0.1 g), moderate (53–56 s, 0.3 g) and severe (56–59.5 s, 0.9 g). The velocity-time curve and total braking force demand are also plotted in the figure. During the severe stage, emergency braking is triggered (orange curve) after the brake strength (z) exceeds 0.6 g.

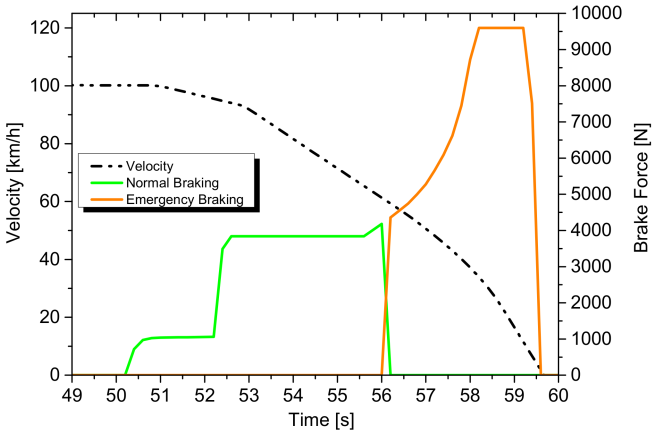

Figure 15. Braking force distribution of the straight braking test cycle.

Figure 16 presents the brake test results for the ECO strategy, which are plotted with the braking force distribution and vehicle velocity-time curve. During the soft braking stage, the motor provided the entire braking force (green line). When the mid-braking stage occurred, the motor's braking force reached its maximum value, and both front and rear mechanical brakes (the orange and light blue lines) were engaged, based on the ECE regulation curve (Figure 8). Regarding the emergency braking stage, regenerative braking quickly stopped and was replaced by complete mechanical braking, according to the ideal braking force distribution.

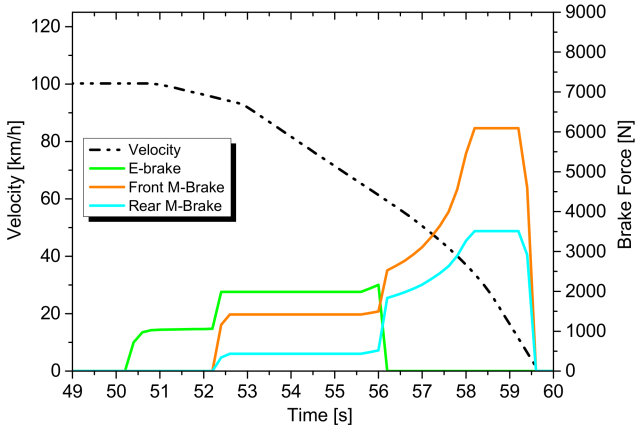

Figure 16. Braking force distribution in the ECO strategy.

As shown in Figure 17, the serial strategy differed from the ECO strategy and strictly followed the ideal braking force distribution. Motor braking (described as "E-brake" in the figures) and rear mechanical braking simultaneously functioned in the soft and mid-braking stages, based on the ideal braking force distribution. When emergency braking occurred, the motor braking was replaced by mechanical braking, to provide a safer braking performance.

The racing strategy, which is plotted in Figure 18, had a higher balanced and dynamic distribution. To adjust to all types of braking situations, the ratio of front wheel braking distribution differed according to various factors. In the soft braking stage, the vehicle speed was high at 100 km/h and the braking command was soft, as the regenerative braking provided most of the braking force (corresponding to a maximum force of 9:1). The contribution of front mechanical braking increased when the vehicle speed decreased at the mid-braking stage. The rear mechanical braking continued to work to ensure safety during aggressive driving. In the case of emergency braking, the racing strategy operated identically to the remaining two strategies.

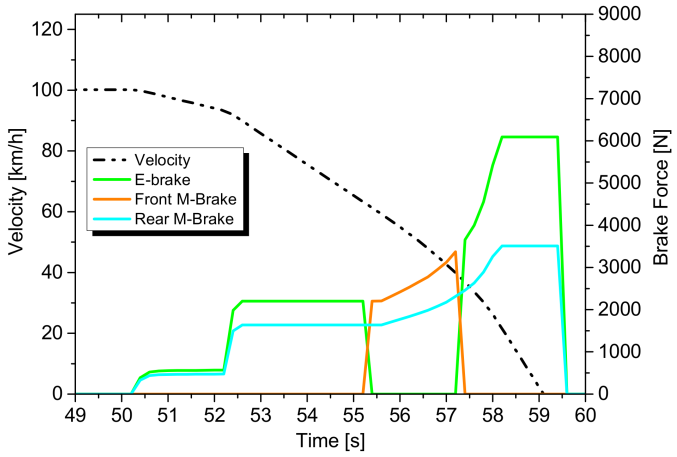

Figure 17. Braking force distribution in the serial strategy.

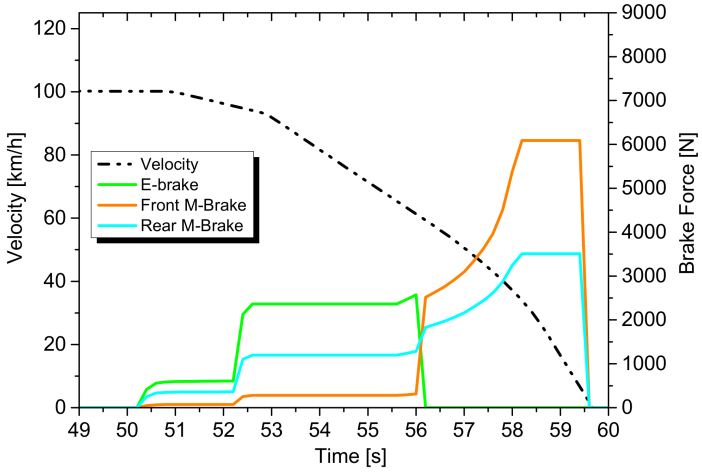

Figure 18. Braking force distribution in the racing strategy.

The three strategies have their own advantages and shortcomings. The ECO strategy has the highest recovery ability, particularly during the soft and mid-braking stage; however, its braking safety should be considered. The safety strategy has a stable braking structure to reduce the possibility of slipping, by maintaining fixed-ratio mechanical braking at all wheels, and has an acceptable energy recovery performance during normal driving circumstances. However, the first two strategies cannot be automatically adapted to vehicle velocity and offer no protection against battery overcharging. Therefore, the racing strategy is proposed. Its regenerative performance can rapidly change according to all circumstances, which indicates that the strategy has the ability to handle all types of aggressive driving while ensuring smooth and safe regenerative braking.

4.2. Driving Cycle Test

The driving cycle economic test was based on two typical city cycles and one experimental cycle in Shenzhen. These three driving cycles may represent the majority of the urban road conditions in Europe, the USA and China, such as urban cycles, highway cycles, high-acceleration driving and traffic jam situations.

Figure 19a, Figure 20a, Figure 21a show the speed-time data of various cycles and the wheel driving/braking force variations. The speed-time data are denoted by a black solid line on the left Y-axis, while wheel force variation is plotted in red on the right Y-axis.

Figure 19b, Figure 20b, Figure 21b demonstrate the relationship between travel distance and battery consumption of travel, based on various braking strategies. The lines of the strategies begin at the same point, as a vehicle starts with 50% of the battery SOC. The NoRegen line is used as a baseline, and the green line, blue line, and red line represent the ECO strategy, serial strategy and racing strategy, respectively. The left Y-axis represents the battery SOC, and the four coloured lines represent its trends. The travel distance is plotted as a dashed-dotted line referred to the right Y-axis.

NEDC was constructed with four straight standard acceleration cycles and one highway cycle. As shown in Figure 19, the acceleration and deceleration were high, which indicates that a large amount of energy was consumed in the braking system. Therefore, the ECO strategy can recover a large amount of braking power in this cycle efficiently, followed by the racing strategy and the serial strategy. The racing strategy efficiently works with this aggressive speed and high deceleration.

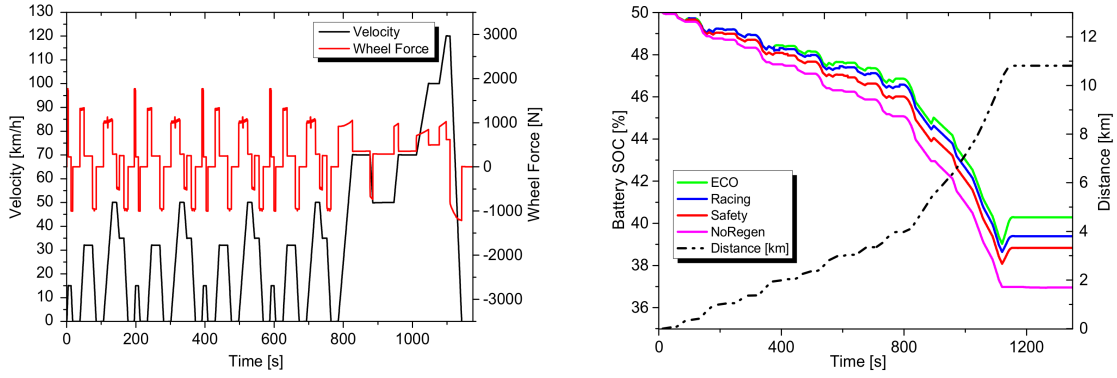

Figure 19. (**a**) Wheel horizontal braking force in NEDC; (**b**) economy simulation results for each strategy.

Using real-world measurements as the data collection method, the SZDC driving pattern is similar to FTP75 and LA92. In Figure 20, we show the comparison of strategies based on SZDC. The ECO strategy yielded the best regenerative energy performance. The energy recovery of the racing strategy and serial strategy were almost equivalent. However, the SOC trend without regenerative braking descended more quickly than the SOC trend with regenerative braking, which suggests that both strategies continue to work in highly efficient conditions.

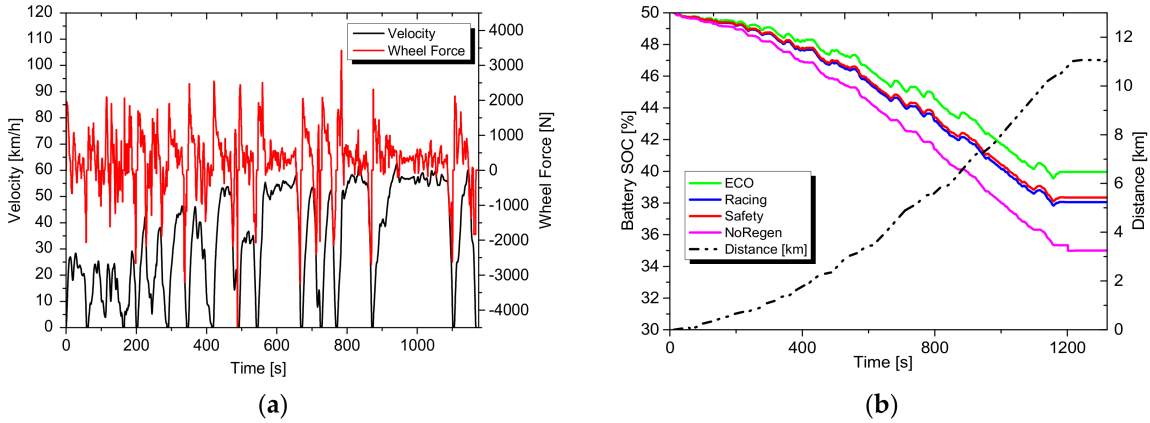

Figure 20. (**a**) Wheel horizontal braking force in SZDC; (**b**) economy simulation results for each strategy.

As shown in Figure 21, LA92 is constructed of low-speed paragraphs that share a steady driving pattern. The racing strategy continued to follow the serial strategy's performance, whereas the ECO strategy yielded the best performance. The NoRegen line deviated from the other lines and created a larger gap than the states in SZDC.

A comparison of the battery SOC trends, based on various strategies, revealed features of the strategies. For steady and low-speed driving cycles, the ECO strategy is highly recommended for its full recovery. To guarantee the anti-slipping ability for high-speed driving or slippery roads, the serial strategy should be selected. When a driver wants to enjoy driving a fast car, the racing strategy provides safe and high recovery braking control during the intense acceleration and braking.

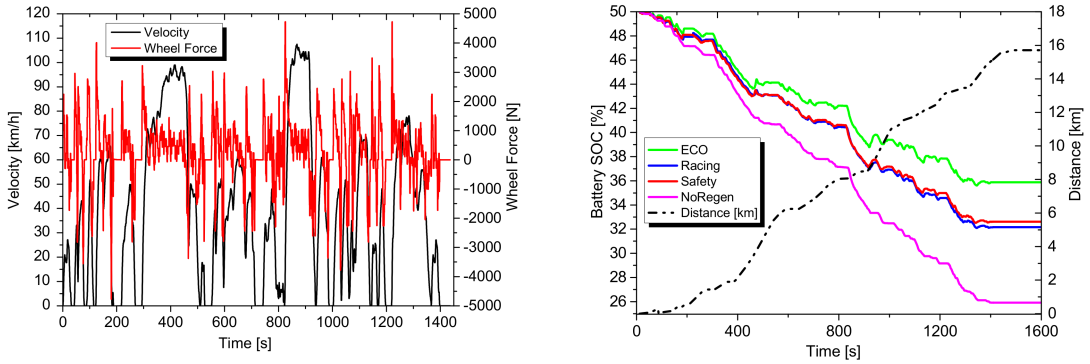

(**a**) (**b**)

Figure 21. (**a**) Wheel horizontal braking force in LA92; (**b**) economy simulation results for each strategy.

Comprehensive simulations of recovery potential were tested on common driving cycles. The results, which are shown in Figure 22, indicated that the proposed strategies are efficient. The ECO strategy yields the highest recovery rate. The majority of the braking force is provided by regenerative braking in this strategy. The serial strategy is next. Causing vehicle stabilization, the serial strategy continuously distributes some of the braking force to the rear mechanical braking, which produces a lower recovery rate. Compared with these two strategies, the racing strategy provides a desirable recovery performance, without compromising the stability issue. Using a multi-input fuzzy controller, real-time signals can contribute to the ideal condition adjustment of regenerative braking. The racing braking strategy may gain a higher recovery rate in cycles with high-speed and aggressive driving micro-trips. Therefore, a driver should select the proper strategy based on the circumstances to achieve a higher performance.

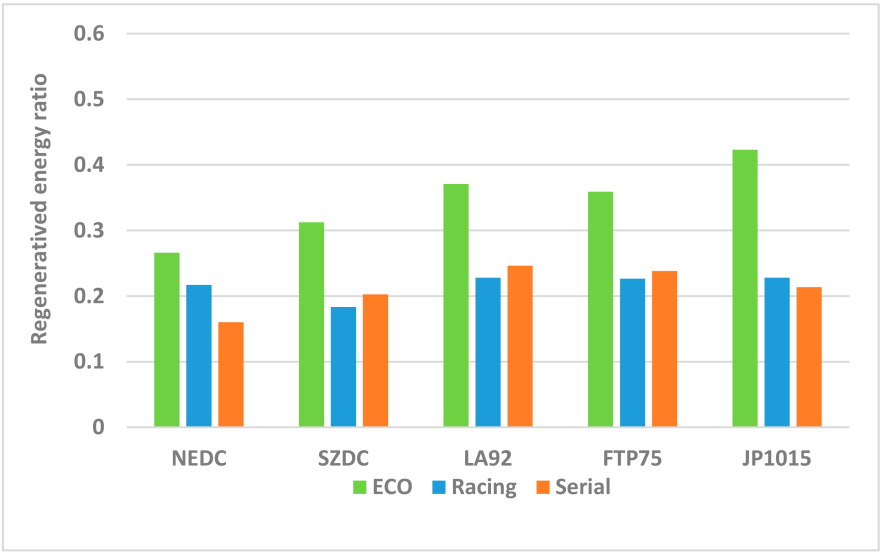

Figure 22. RBS recovery potentials in various driving cycles.

5. Conclusions

We have discussed distinctive strategies of regenerative braking distribution. Braking restriction rules were accounted for in the model. A methodology of the China urban driving cycle was developed, using micro-trips extracted from real-world driving data and compared with standard cycles in the BEV model simulation. Electric motor and battery models were established, based on experimental data.

Three regenerative braking strategies, namely, "ECO", "racing", and "serial", underwent comparison testing. The segmented straight braking test and energy recovery potential test were performed; the results indicated excellent braking safety and a favourable recovery rate from these braking distribution methods. During the recovery economic potential test, the ECO strategy had the highest energy recaptured by a powerful motor, which provided most of the cycles for the entire braking force. For example, the ECO strategy recaptured almost 42% of the energy at the JP1015 cycle; however, this strategy is inadequate on slippery roads. The racing strategy, using a multi-input fuzzy logic controller, quickly adapts to all driving conditions and achieved a balanced braking performance: 21.1% and 22.7% for NEDC and JP1015, respectively.

The results demonstrate the different characteristics of the proposed strategies and confirm the feasibility and potential of the proposed RBS strategies catering to the braking demands of BEVs. This study provides a comprehensive reference on energy recovery possibilities for manufacturers and scholars.

Acknowledgments: This study was conducted with the financial support of the National Key Research and Development Program of China (Program No. 2016YFD0701100). Boyi Xiao is grateful for the support from South China Agricultural University and the University of Technology Sydney.

Author Contributions: Boyi Xiao designed the fuzzy-based control strategy and performed the driving cycle construction and the simulation analysis. Jiageng Ruan and Hailin Wang proposed the two referential strategies and guided the design of the BEV model. Huazhong Lu and Nong Zhang supervised the research. All authors contributed to the writing of this paper.

Conflicts of Interest: The authors declare no conflict of interest.

References

1. Metz, L.D. Potential for passenger car energy recovery through the use of kinetic energy recovery systems (KERS). In Proceedings of the SAE 2013 World Congress & Exhibition, Detroit, MI, USA, 16–18 April 2013; SAE: Warrendale, PA, USA, 2013. [CrossRef]
2. Paganelli, G.; Ercole, G.; Brahma, A. General supervisory control policy for the energy optimization of charge-sustaining hybrid electric vehicles. *JSAE Rev.* **2001**, *22*, 511–518. [CrossRef]
3. Gao, Y.; Ehsani, M. Electronic Braking System of EV and HEV-Integration of Regenerative Braking, Automatic Braking Force Control and ABS. Available online: https://doi.org/10.4271/2001-01-2478 (accessed on 3 December 2014).
4. Crolla, D.A.; Cao, D. The impact of hybrid and electric powertrains on vehicle dynamics, control systems and energy regeneration. *Veh. Syst. Dyn.* **2012**, *50*, 95–109. [CrossRef]
5. Oleksowicz, S.A.; Burnham, K.J.; Southgate, A.; McCoy, C.; Waite, G.; Hardwick, G.; Harrington, C.; McMurran, R. Regenerative braking strategies, vehicle safety and stability control systems: Critical use-case proposals. *Veh. Syst. Dyn.* **2013**, *51*, 684–699. [CrossRef]
6. Zhang, J.; Lv, C.; Qiu, M.; Li, Y.; Sun, D. Braking energy regeneration control of a fuel cell hybrid electric bus. *Energy Convers. Manag.* **2013**, *76*, 1117–1124. [CrossRef]
7. Xiao, B.; Zeng, X.; Zhang, Z.; Li, B.; Yang, Y. Present status and prospect of the regenerative-braking control strategies of electric automobiles. *Auto Electr. Parts* **2016**, *12*, 1–3. [CrossRef]
8. Martin, R.; Richard, A.U.; Tilo, K.; Markus, L. Combining Regenerative Braking and Anti-Lock Braking for Enhanced Braking Performance and Efficiency. In Proceedings of the SAE 2012 World Congress & Exhibition, Detroit, MI, USA, 24–26 April 2012; SAE: Warrendale, PA, USA, 2012. [CrossRef]
9. Juan, J.C.A.; Javier, P.F.; Juan, M.V.G.; Juan, A.C.C. Regenerative Intelligent Brake Control for Electric Motorcycles. *Energies* **2017**, *10*, 1648. [CrossRef]

10. *Regulation No. 13-H: Uniform Provisions Concerning the Approval of Passenger Cars with Regard to Braking*; United Nations: New York, NY, USA, 2014; Volume 97. Available online: https://treaties.un.org/Pages/ViewDetails.aspx?src=TREATY&mtdsg_no=XI-B-16-13H&chapter=11&lang=en&clang=_en (accessed on 25 March 2014).
11. National Highway Traffic Safety Administration. *Laboratory Test Procedure for 2005*; National Highway Traffic Safety Administration: Washington, DC, USA, 2005.
12. ECE15+EUDC/NEDC Emission Test Cycles. Available online: https://www.dieselnet.com/standards/cycles/ece_eudc.php (accessed on 15 December 2016).
13. EPA U. LA92 Unified Dynamometer Driving Schedule/Emission Standards Reference Guide/US. Available online: https://www3.epa.gov/otaq/standards/lightduty/la92.htm (accessed on 2 March 2017).
14. Duran, A.; Earleywine, M. GPS data filtration method for drive cycle analysis applications. In Proceedings of the SAE 2012 World Congress & Exhibition, Detroit, MI, USA, 24–26 April 2012; SAE: Warrendale, PA, USA, 2012. [CrossRef]
15. Justin, D.K.; Axon, C.J. A robust, data-driven methodology for real-world driving cycle development. *Transp. Res. Part D Transp. Environ.* **2012**, *17*, 389–397.
16. Kamble, S.H.; Mathew, T.V.; Sharma, G.K. Development of real-world driving cycle: Case study of Pune, India. *Transp. Res. Part D Transp. Environ.* **2009**, *14*, 132–140. [CrossRef]
17. Hung, W.T.; Tong, H.Y.; Lee, C.P.; Ha, K.; Pao, L.Y. Development of a practical driving cycle construction methodology: A case study in Hong Kong. *Transp. Res. Part D Transp. Environ.* **2007**, *12*, 115–128. [CrossRef]
18. Haan, P.D.; Keller, M. *Real-World Driving Cycles for Emission Measurement: ARTEMIS and Swiss Cycles*; Final Reports; ResearchGate: Berlin, Germany, 2001.
19. Hongwen, H.; Rui, X.; Jinxin, F. Evaluation of Lithium-Ion Battery Equivalent Circuit Models for State of Charge Estimation by an Experimental Approach. *Energies* **2011**, *4*, 582–598. [CrossRef]
20. Ruan, J.; Walker, P.D.; Watterson, P.A.; Zhang, N. The dynamic performance and economic benefit of a blended braking system in a multi-speed battery electric vehicle. *Appl. Energy* **2016**, *183*, 1240–1258. [CrossRef]
21. Genta, G.; Morello, L. *The Automotive Chassis Volume 2: System Design*; Springer: Dordrecht, The Netherlands, 2009; pp. 239–240, ISBN 978-1-4020-8673-1.
22. Ehsani, M.; Gao, Y.; Ali, E. *Modern Electric, Hybrid Electric and Fuel Cell Vehicles: Fundamentals, Theory, and Design*, 2nd ed.; CRC Press: Boca Raton, FL, USA, 2009; ISBN 9781420053982.
23. Zadeh, L.A. Fuzzy sets. *Inform. Contr.* **1965**, *8*, 338–353. [CrossRef]
24. Michels, K.; Klawonn, F. *Fuzzy Control: Fundamentals, Stability and Design of Fuzzy Controllers*; Springer: Berlin/Heidelberg, Germany, 2006; Volume 200, pp. 1–5, 243–245.
25. Hájek, P. *Metamathematics of Fuzzy Logic*, 4th ed.; Springer: Dordrecht, The Netherlands, 1998; Chapter 4, pp. 35–45.